AGU100 ADVANCING EARTH AND SPACE SCIENCE

Tectonics

RESEARCH ARTICLE
10.1029/2017TC004780

Special Section:
The 2016 Central Italy Seismic Sequence: Insights, implications and lessons learned

Evidence for Surface Faulting Earthquakes on the Montereale Fault System (Abruzzi Apennines, Central Italy)

F. R. Cinti[1], R. Civico[1], A. M. Blumetti[2], E. Chiarini[2], E. La Posta[2], D. Pantosti[1], F. Papasodaro[2], A. Smedile[1], P. M. De Martini[1], F. Villani[1], S. Pinzi[1], S. Pucci[1], and C. A. Brunori[1]

[1]Istituto Nazionale di Geofisica e Vulcanologia, Rome, Italy, [2]Istituto Superiore per la Protezione e la Ricerca Ambientale, Rome, Italy

Key Points:
- Seven earthquakes ruptured the Montereale fault system (central Italy) since 26 kyr
- First estimates of the Montereale fault parameters: length, earthquake recurrence, and slip rate
- The Montereale fault system is an individual earthquake source within the central Apennines seismogenic belt (Italy)

Supporting Information:
- Supporting Information S1

Correspondence to:
F. R. Cinti,
francesca.cinti@ingv.it

Citation:
Cinti, F. R., Civico, R., Blumetti, A. M., Chiarini, E., La Posta, E., Pantosti, D., et al. (2018). Evidence for surface faulting earthquakes on the Montereale fault system (Abruzzi Apennines, central Italy). *Tectonics*, *37*. https://doi.org/10.1029/2017TC004780

Received 28 AUG 2017
Accepted 7 AUG 2018
Accepted article online 17 AUG 2018

Abstract We conducted paleoseismic studies along the Montereale fault system (MFS; central Italy). The MFS shows geomorphological evidence of Late Quaternary activity and falls within the highest seismic hazard zone of central Apennines, between the epicentral areas of two recent earthquake sequences: 2009 L'Aquila and 2016–2017 central Italy. We excavated two trenches along the San Giovanni fault splay of the system, one intercepting the N140° striking bedrock main fault plane and the other cutting two subparallel fault scarps on the colluvial/alluvial deposits on the fault hanging wall. Excavations revealed repeated fault reactivation with surface faulting in prehistorical and historical times. We recognized and dated seven events in the last 26 kyr. The most recent ground-rupturing event (evb1) possibly occurred 650–1,820 AD, consistent with one of the three main shocks that struck the area in 1,703 AD. A previous event (evb2) occurred between 5,330 BC and 730 BC, while older events occurred at 6,590–5,440 BC (evb3), 9,770–6,630 BC (evb4), and 16,860–13,480 BC (evb5). We documented two older displacement events (evb7 and evb6) between 23,780 BC and 16,850 BC. The minimum vertical slip rate at the trench site in the last 28–24 kyr is 0.3–0.4 mm/year. The inferred average recurrence interval for surface-faulting events along the MFS is no longer than ~4 kyr. Based on the surface fault length ranging between 12 and 20 km, earthquakes with $\geq M$ 6.0 are possible for the MFS. The MFS is an independent earthquake source, and its paleoseismic data are fully comparable with those known for faults in central Apennines.

1. Introduction

The Montereale fault system (MFS; Figure 1) belongs to a dense array of NW-SE striking, mainly normal faults accommodating the present-day ~1–3 mm/yr regional NE-SW extension of the central Apennines (D'Agostino et al., 2008, 2011; Devoti et al., 2011; Faure Walker et al., 2010). In particular, significant gradients of northeastward directed GPS velocities are observed across and in the vicinity of the MFS (D'Agostino et al., 2011). The prevalent normal slip activity of the MFS is responsible for the evolution of the intermontane Montereale Basin (Figure 1), and contributed to the basin-and-range setting that is a common morphotectonic feature in the Apennines (Blumetti et al., 1993; Blumetti & Guerrieri, 2007; Cavinato and De Celles, 1999; Cello et al., 1997; Galli et al., 2005).

The MFS has a complex fault structure at the surface, and it is composed of the subparallel, down-to-the-west Capitignano fault (CF) and San Giovanni fault (SGF) main faults with an average strike of N145° (Figure 2), characterized by a normal slip kinematic with a minor left-lateral component (Chiarini et al., 2014; Civico et al., 2016; Lavecchia et al., 2012). In Blumetti (1995), the CF was pointed out as recently active based on the occurrence of fault scarps on Middle Pleistocene alluvial fan deposits; later on, Lavecchia et al. (2012) considered the CF and the SGF to belong to the same fault system acting as an independent extensional source on the basis of instrumental seismicity. The Montereale intermontane basin has been the subject of specific Quaternary geology studies and of focused research on the activity of the CF and SGF during the survey of the 1:50,000 scale official geological map (Chiarini et al., 2014). Recently, Civico et al. (2016) accurately mapped the traces of the CF and SGF using LiDAR Digital Terrain Model and field data (Figure 2), providing also geomorphological and shallow geophysical constraints testifying to their repeated activity during the Late Pleistocene-Holocene period. However, the CF and SGF behavior and interaction have been only partially defined, their Holocene activity not documented, and their seismic potential not assessed.

10.1029/2017TC004780

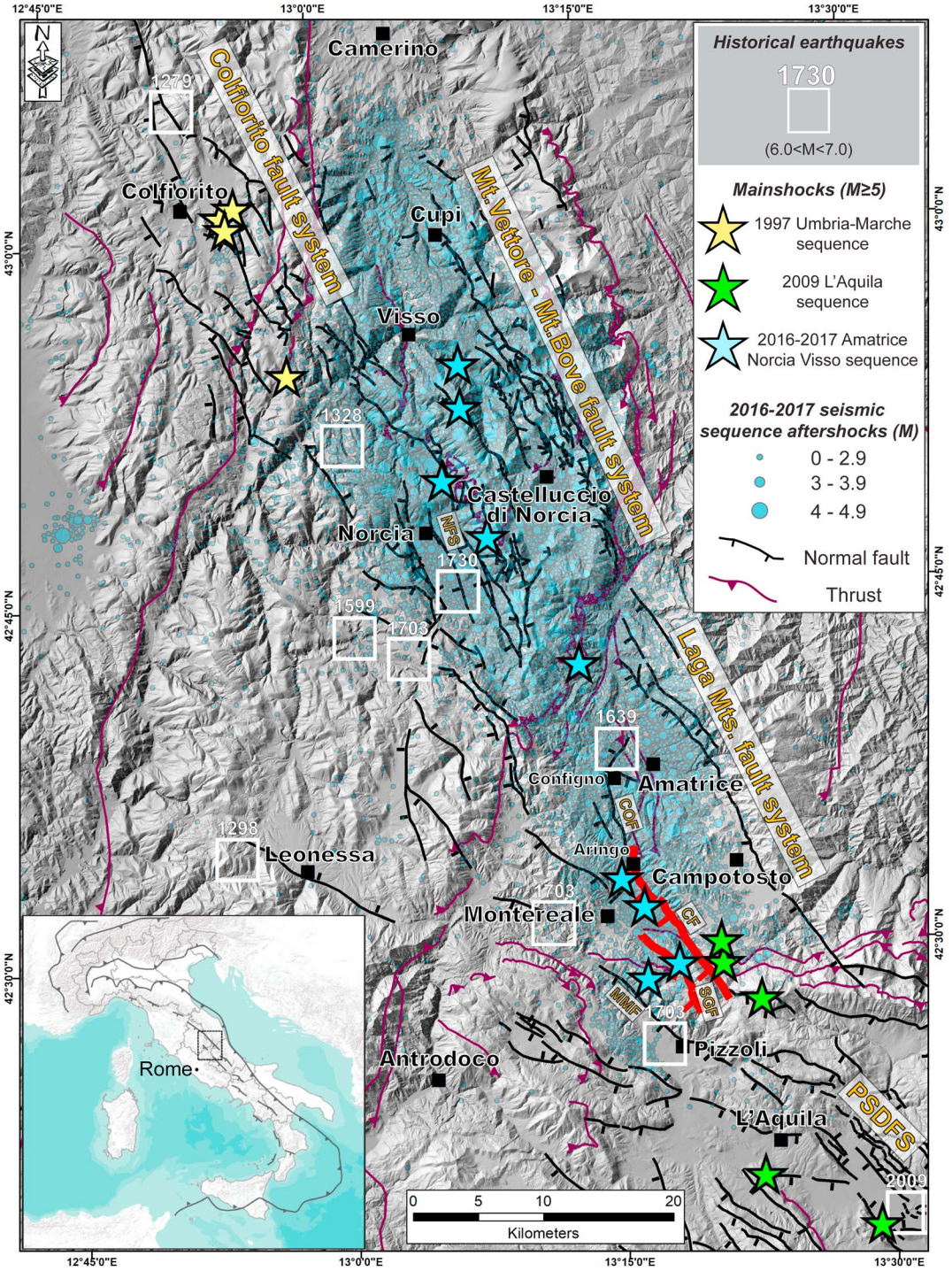

Figure 1. Map of the $M \geq 5$ mainshocks of the 2016–2017 central Italy (blue stars), 2009 L'Aquila (green stars), and 1997 Umbria-Marche (yellow stars) seismic sequences. The 2016–2017 aftershocks (blue circles scaled to magnitude) are also shown (until 23 January 2017; data from ISIDE http://iside.rm.ingv.it). Date and location of the macroseismic epicenters of the moderate-large historical earthquakes (Guidoboni et al., 2018) are reported with white squares. The major active normal faults in the area (modified after Centamore et al., 1992; Festa, 2005; Galadini & Galli, 2000; Pierantoni et al., 2013; Pucci et al., 2015; Vezzani & Ghisetti, 1998) are traced with black lines. The names of the fault systems activated during the three seismic sequences are indicated: from southeast to northwest, Paganica-S. Demetrio (PSDFS) in 2009, southern portion of the Laga Mountains in 2017, and northern portion of the Laga Mountains and Mount Bove-Mount Vettore in 2016 and Colfiorito in 1997. The Capitignano (CF) and San Giovanni (SGF) faults compose the Montereale fault system (MFS) and are shown in thick red lines. MMF = Mount Marine fault, NFS = Norcia fault system, COF = Configno fault.

The MFS falls within the zone of highest seismic hazard of central Apennines (available at http://zonesismiche.mi.ingv.it/). Moderate to large earthquakes dramatically devastated this territory both in the historical and in recent times (Figure 1; Chiarabba et al., 2005; Guidoboni et al., 2018). In 1703, three major events of local intensity ranging from VIII to X Mercalli-Cancani-Sieberg occurred in a cascade mode within about half a month on different faults from the Norcia village to the north, passing through the Montereale area, down south to the town of L'Aquila (Blumetti, 1995; Cello et al., 1998; Galli et al., 2005; Guidoboni et al., 2018). A scenario of multiple shocks and activation of different faults replayed on April 2009 when three main shocks up to M_w 6.1 struck in 4 days the town of L'Aquila and its surroundings (Chiaraluce et al., 2011). Then nine $M \geq 5.0$ earthquakes, culminating with a M_w 6.5, occurred in succession from 24 August 2016 to 18 January 2017 (reports available at terremoti.ingv.it/it/ultimi-eventi/; Chiaraluce et al., 2017; INGV Working Group, 2016; Gruppo di Lavoro INGV sul terremoto di Visso, 2016; Gruppo di Lavoro INGV sul terremoto in centro Italia, 2016, 2017) in the eastern fault array of the central Apennines, around the villages of Visso, Castelluccio, Amatrice, and down to Campotosto (Figure 1). The 2009 L'Aquila and the 2016–2017 central Italy earthquakes were concentrated in a NW-SE alignment from north to south and definitively testified that we need to cope with the occurrence of multiple main shocks close in space and time on adjacent faults.

Although we cannot predict the development of a sequence in time, we have the tools and know-how for predicting the possible scenarios of spatial fault triggering in this portion of the Apennines. The Montereale fault system lies in the middle of the complex tectonic area, not releasing energy during the recent seismic crisis but being a possible candidate source for one of the 1703 events (Boncio et al., 2004).

The definition of the rupture history of the MFS is a mandatory issue for evaluating the seismic hazard of the region and that associated with surface fault rupture. In order to contribute to this aim, we performed a trenching campaign across the SGF scarp in 2015–2016. Here we present the first paleoseismic data and analysis of the seismic behavior of the system, also discussing its setting and role in the framework of the recent seismic sequence striking central Italy.

2. Paleoseismic History of the Montereale Fault

Both the CF and the SGF surface expression comprise 200- to 800-m-wide deformation zones with multiple subparallel, locally overlapping traces (Figure 2). The ~12-km-long CF trace runs at the base of a prominent mountain front (highest peak Civitella Mountain 1,603 m above sea level) characterized by wine-glass valleys, well-defined triangular facets (occurring mainly in the synorogenic siliciclastic deposits of the Laga formation), drainage anomalies, fault scarps in Quaternary deposits of different ages, and by rare outcrops of the bedrock fault plane (Figure S1; Chiarini et al., 2014; Lavecchia et al., 2012). A potential northward extension of the CF can be identified in the N170° striking, ~7-km-long Configno normal fault, between the Aringo and Configno villages (COF; Figure 1; Festa, 2005; Lavecchia et al., 2012). The ~8-km-long SGF trace, which lies ~2–3 km west of the CF, bounds the SW slope of the Meso-Cenozoic basin-to-slope carbonate succession of Mount Mozzano, giving rise to a straight fault scarp with a well-exposed bedrock fault plane (Figure S1).

We found the most favorable conditions (i.e., narrow zone of deformation, young deposits) for paleoseismological trenching investigations along the SGF (Figures 2 and 3) at the mouth of the Grande creek valley, at the northern end of the Mount Mozzano ridge. We used subsurface imaging from shallow geophysical campaigns (Civico et al., 2016) to infer the location of fault zones and thus for trench positioning. Furthermore, the selected site was an opportunity to merge the information acquired by us in 2005 from a temporary exposure of the SGF fault zone within a nearby quarry (Figure 3).

2.1. The SGF Zone at the Quarry Site

In 2005, an ~4-m-high and ~25-m-long quarry wall showed the northern portion of the SGF ~3 m below the present-day surface (Figures 3 and 4). Here the SGF is expressed by a complex NW-SE trending fault zone consisting of five parallel fault strands (F1 to F5), cutting both the bedrock (units 11 to 15), the paleosols, and the alluvial and debris deposits (units 2 to 10) filling the Grande creek valley (Figure 4). The eastern three fault strands (F1, F2, and F3) affect the bedrock, made up of limestones (Scaglia Bianca formation, Upper Cretaceous-Eocene p.p.) and marls (Scaglia Cinerea formation, Eocene p.p.-Oligocene) of a basin-to-slope carbonate succession (Centamore et al., 1992). The very steep attitude of the strata belonging to the Scaglia

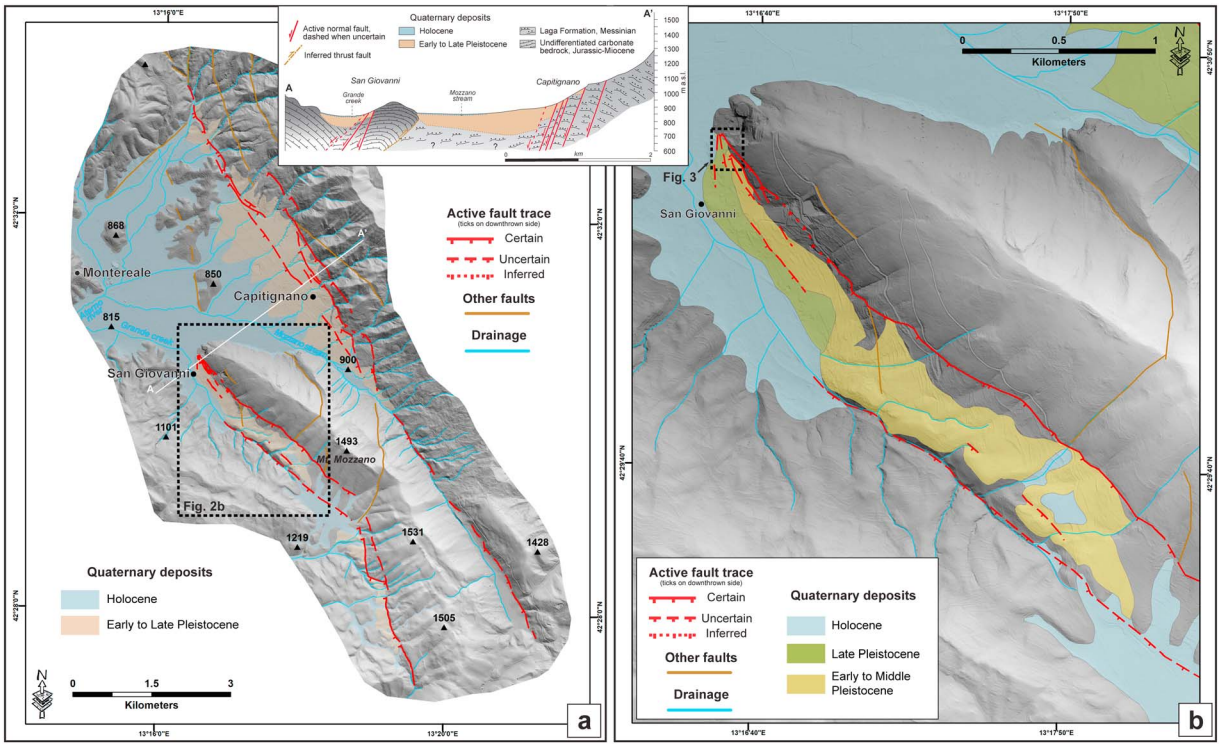

Figure 2. (a) Map of the active traces of the Capitignano (CF) and San Giovanni faults (SGF) in the area of the Montereale basin (central Apennines, Italy; modified after Civico et al., 2016). The inset in the top right shows a schematic geological section across the Montereale intermountain basin (vertical exaggeration 2X; A-A′ trace reported in the map as white line). Bedrock data are modified from Vezzani and Ghisetti (1998). (b) Map of the SGF active traces and distribution of the outcropping Quaternary continental deposits in the vicinity of the SGF. LiDAR DTM as base imagery.

Cinerea formation at the hanging wall of F1 and their pervasive folding between F2 and F4 suggest a thrust style of deformation. On the other hand, it is well known that this area, like the whole Apennine Chain, experienced a poly-phasic tectonics, where Quaternary extension followed an upper Miocene to Middle Pliocene compressional tectonic phase. F4 brings in contact the bedrock with weathered, strongly deformed Quaternary alluvial and debris deposits, presumably Late Pleistocene in age. F5 cuts between these deposits and less deformed alluvial deposits that yielded ages of 28,740–27,620 BC (CL18–15) and 29,230–28,800 BC (BCAVE) from ^{14}C analysis of bulk samples (Table 1). West of F5 an ~1.5-m-wide fissure (meters 22–23) is filled with a dark brown silty clay derived from a paleosol (unit 3) dating back to 32,500–31,550 BC (CL18A; Table 1). We interpret the infill as a coseismic feature. The paleosol, unit 3 (partly concealed by the quarry waste deposits, unit 1; Figure 4a), covers the deformed deposits of the quarry exposure with a minimum thickness of 2.5 m. Unit 3 was dated at 31,960–30,890 BP (CL18B; Chiarini et al., 2014). It is not possible to identify discrete events horizons of surface faulting in the quarry exposure. Furthermore, the radiocarbon datings on bulk sediment are not in stratigraphic order, then revealing accuracy problems. Nevertheless, the structural setting, the intense deformation of the stratigraphy, and the chronological context point to repeated tectonic activity of the SGF in the Late Pleistocene.

2.2. The San Giovanni Trenches: Setting and Stratigraphy

At the end of 2015, we excavated two trenches across the northwestern part of the SGF (Figures 2 and 3): SG1 intercepting the N140° striking bedrock main fault plane and SG2 cutting across two subparallel subtle fault scarps on the colluvial and alluvial deposits on the main fault hanging wall. Trenches overlap for ~1 m, their strike diverges less than 10°, and they are ~4 m apart. They were excavated 50 m to the south, outside the quarried zone, along the same strike and at a ground level ~7 m higher than the quarry exposure (Figures 3 and 4).

Trenches SG1 and SG2 exhibit the depositional, erosional, and deformational history of the site in the last ~30 kyr (Table 1). This age interval is constrained by a total of 24 accelerator mass spectrometry carbon

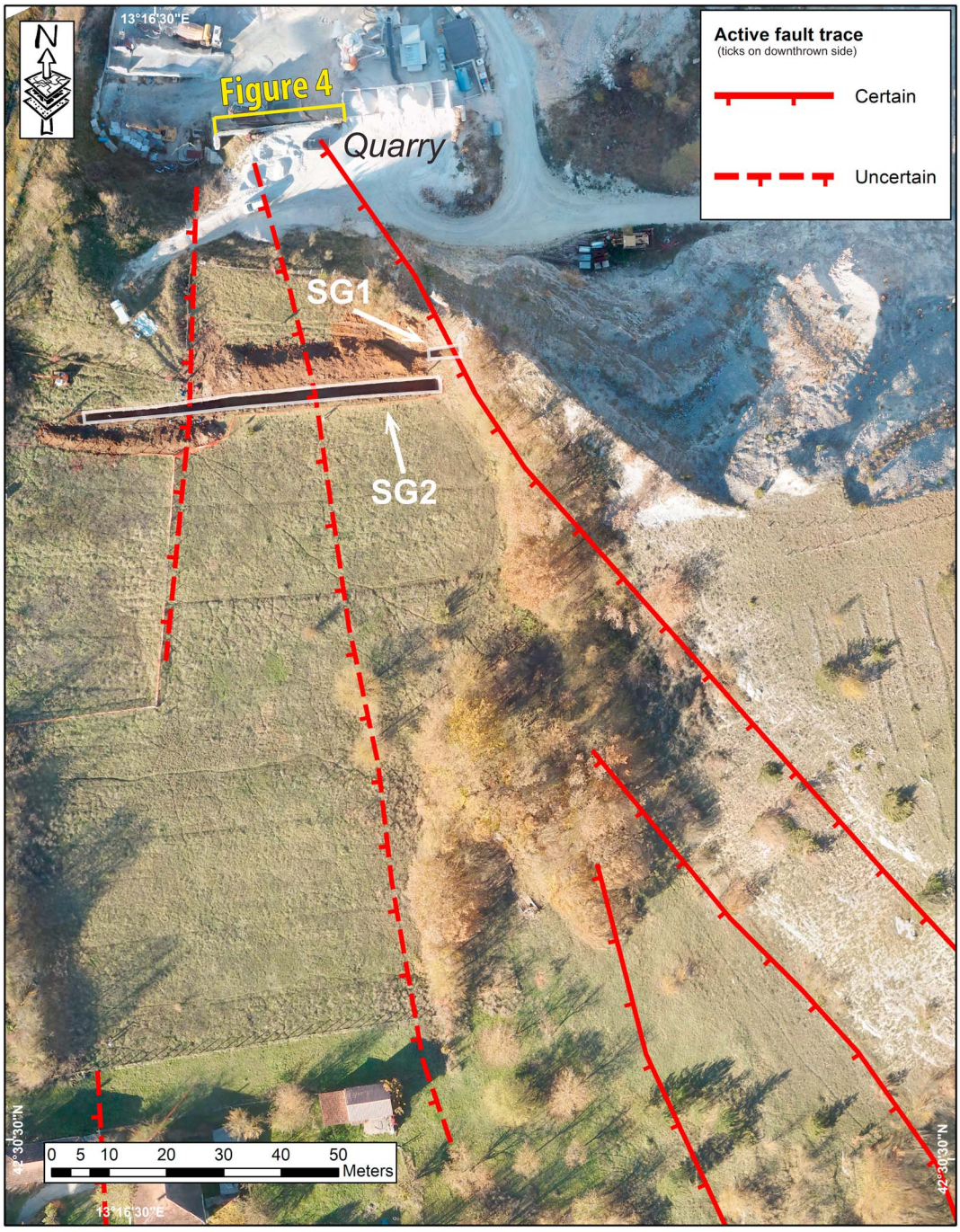

Figure 3. Ortophotomosaic of the SG1 and SG2 trench site generated by structure-from-motion (SfM) photogrammetry from balloon platform. White arrows point to the excavations. Red lines are the fault traces, and mark the base of the morphological scarps. Location of the SGF zone exposed in a former quarry wall and shown in Figure 4 is also indicated.

dating of bulk (organic sediment) and charcoal (plant-related charred material) samples submitted at different laboratories (Table 1). Standard pretreatments were used: acid washes for organic sediment and acid/alkali/acid for charred material. Moreover, thermoluminescence dating (TL) was applied for three terracotta brick fragments collected within the archeological stratigraphy found in SG2 trench (Table 1).

In both trenches, the SSE and NNW wall exposures are substantially mirrored in terms of stratigraphy and structures. Units that belong to the same depositional event or are found at the same chronological

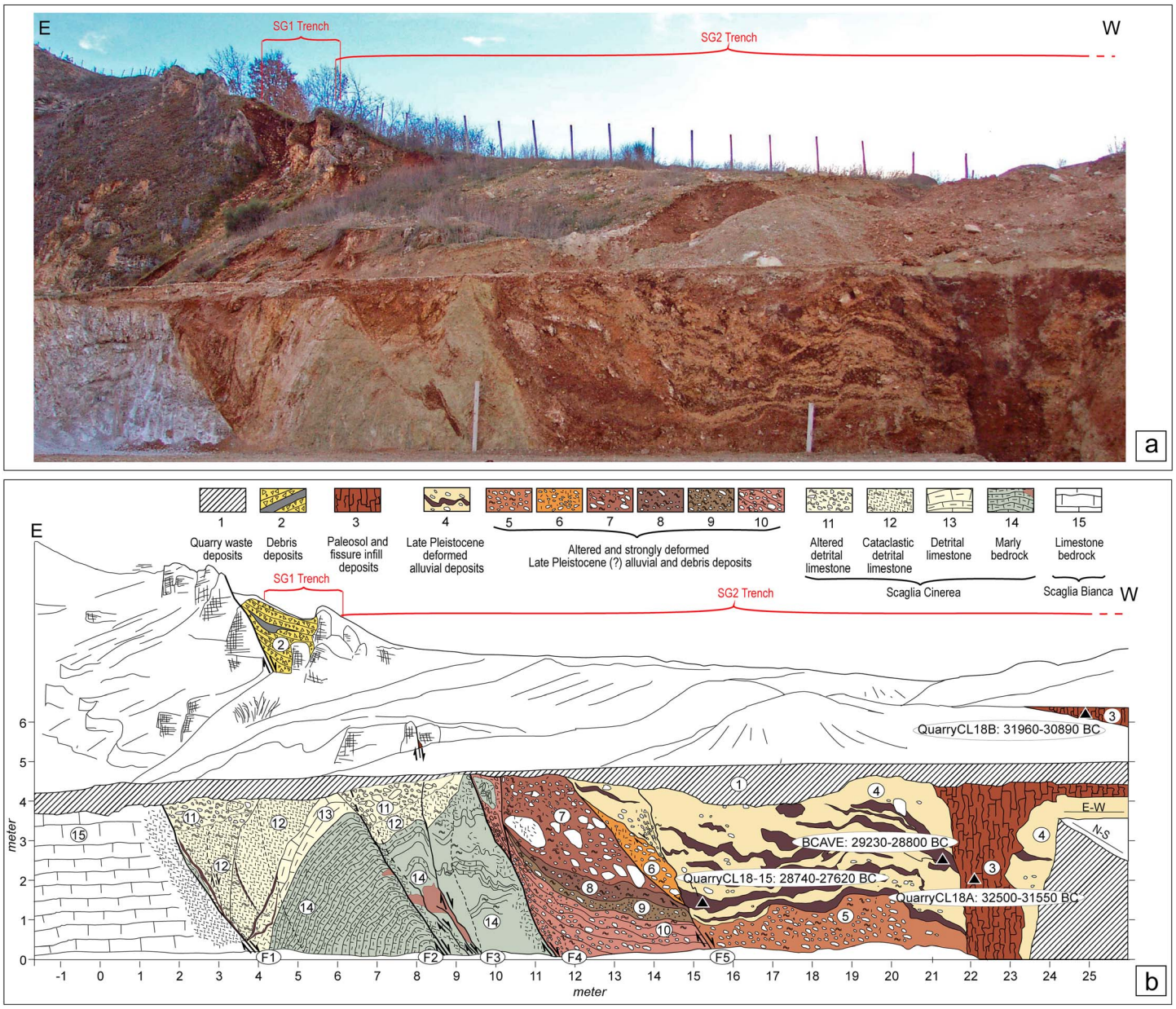

Figure 4. The SGF zone at the quarry site (view to the south). A complex fault zone was exposed on the 4-m-high, 25-m-long quarry wall (not visible anymore; Figure 3). This exposure was about 50 m north of and 7 m below the position of SG1-SG2 trenches (red arrowed lines indicate projected extent of trenches; see also Figure 3 for location). (a) Photo of the fault zone showing the deformed Late Pleistocene sedimentary sequence. (b) Log of the fault zone and ^{14}C ages of the samples collected (see Table 1). All samples are bulks that were processed soon after their sampling between 2007 and 2013. Sample quarry CL18B was already reported in Chiarini et al. (2014). The deformed layer unit 3 is interpreted as parent material of the colluvial deposit unit Cva exposed in trench SG1 (see Figure 5). Up to meter 6, the exposure was not reachable, so that unit 2 was only observed from remote. Scaglia Bianca and Scaglia Cinerea formations are of Upper Cretaceous-Eocene p.p. and Eocene p.p.-Oligocene age, respectively (Centamore et al., 1992).

position in both trenches are indicated with the same letter and with the same color (units V, Vy1, and A; Figures 5 and 6). The subsurface stratigraphy in the hanging wall of the bedrock fault plane, as exposed primarily in SG2 (Figures 6 and S2), can be described as follows. A strongly consistent carbonate-free silty clay (unit A) and its pedogenized cover (unit A1) are continuous for the first 40 m of the SG2 trench extent. Between meters 32 and 39, units A/A1 overlie unit G, a clast-supported and poorly sorted calcareous gravel. The sedimentary facies association and the vicinity of the Grande creek, presently flowing ~250 m far to the east and maximum 18 m below the units level, suggest that unit A and unit G are both related

Table 1
^{14}C and TL Ages of the Samples Collected in the Trenches and in the Nearby Quarry (°)

Trench-sample code	Sample position (vertical/horizontal)	Unit	Laboratory code[a]	Sample type	$\delta^{13}C$	Conventional age[b] (before 1,950 = B.P.)	Calibrated age[c] (2σ)	Probably distribution
SG2-ISPRA1S	B/3	A1	LTL16355A	Bulk	−32.1	{23,461 ± 120}	25,880–25,480 BC	1.000
SG2-C400N	H/31	A1	Poz-80840	Charcoal	−37.7	{21,100 ± 400}	24,190–22,440 BC	1.000
SG2-B4S	F/21	C2	Poz-80994	Bulk	−33.9	15,210 ± 100	16,770–16,270 BC	1.000
SG2-ISPRA9S	B/9	B	LTL16353A	Bulk	−28.0	{15,621 ± 80}	17,100–16,750 BC	1.000
SG2-C12S	B/2	Vy	Beta-436984	Charcoal	−24.1	22,730 ± 80	25,420–24,800 BC	1.000
SG1-B100N	A/−1	Cva	Beta-431536	Bulk	−24.2	31,020 ± 190	33,420–32,600 BC	1.000
SG1-B103N	A/−3	Cvmix	Beta-431537	Bulk	−23.9	10,900 ± 40	10,880–10,750 BC	1.000
SG1-B101S	B/−3	SS1	Beta-431538	Bulk	−24.1	9,160 ± 30	8,460–8,290 BC	1.000
SG2-B9S	A/2	SS2	Beta-431540	Bulk	−24.3	{12,860 ± 50}	13,550–13,240 BC	1.000
SG2-B5S	D/18	D	LTL16354A	Bulk	−24.4	{10,145 ± 75}	10,110–9,450 BC	1.000
SG2-B23S	E/21	C4	Poz-80783	Bulk	−33.7	{7,780 ± 50}	6,690–6,480 BC	1.000
SG2-B502N	C/12	SS3	Beta-431541	Bulk	−23.9	{6,390 ± 30}	5,470–5,400 BC	0.379
							5,390–5,320 BC	0.621
SG2-B1N	H/34	F	Poz-80779	Bulk	−25.5	{6,420 ± 40}	5,470–5,330 BC	1.000
SG2-B20S	N/57	DS	Beta-436990	Bulk	−24.3	3,770 ± 30	2,290–2,130 BC	0.940
							2,090–2,050 BC	0.060
SG2-F1S	H/37	Ant	Beta-436988	Charcoal	−25.3	{1,730 ± 30}	250–390 AD	1.000
SG2-C5S	L/43	Ant	Beta-436986	Charcoal	−28.2	{1,830 ± 30}	90–110 AD	0.035
							120–250 AD	0.960
SG2-C10S	M/47	Ant	Beta-436989	Charcoal	−24.8	{2,440 ± 30}	590–410 BC	0.645
							750–680 BC	0.246
SG2-C8S	L/40	Ant	Poz-80785	Charcoal	−32.9	{2,190 ± 30}	360–180 BC	1.000
SG2-C1N	I/40	Ant	Beta-436985	Charcoal	−24.5	2,750 ± 30	980–820 BC	1.000
SG2-F2N	M/49	Ant	Beta-436987	Charcoal	−22.5	{1,830 ± 30}	90–110 AD	0.035
							120–250 AD	0.960
SG2-50Nb	L/45	Ant	Fi3203, Fi3207	Charcoal	np	{1,885 ± 50}	10–240 AD	1.000
SG2-B24S	E/21	CD	Poz-80784	Bulk	−31.0	{1,400 ± 30}	600–670 AD	1.000
SG2-C6S	I/43	N	Beta-439198	Charcoal	−24.3	109.8 ± 0.3 pMC	modern	-
SG2-B22S	M/53	N	Beta-439199	Bulk	−25.4	{70 ± 30}	1,690–1,730 AD	0.243
							1,810–1,920* AD	0.711
QuarryCL18B°	6/25	3	LTL1874A	Bulk	−26.2	29,225 ± 250	31,960–30,890 BC	1.000
QuarryCL18A°	2/22	3	LTL13276A	Bulk	−19.2	29,805 ± 270	32,500–31,550 BC	1.000
BCAVE°	3/21	4	Beta-363653	Bulk	−24.6	26,830 ± 140	29,230–28,800 BC	1.000
QuarryCL18–15°	1/15	4	LTL1873A	Bulk	−28.8	25,897 ± 200	28,740–27,620 BC	1.000

Trench-sample code	Sample position (vertical/horizontal)	Unit	Laboratory code	Type	Age TL (before the present day)	Age
SG2-TL2S	I 40	Ant	SG2-TL2S	Brick	{1,535 ± 140}	481 ± 140 AD
SG2-TL3S	H 37	Ant	SG2-TL3S	Brick	1,070 ± 90	961 ± 92 AD
SG2-TL50N	L 45	Ant	SG2-TL50N	Brick	1,180 ± 100	846 ± 100 AD

[a]Laboratory code: Beta, Beta Analytic Radiocarbon Dating Laboratory (FL, USA); LTL, CEntro di DAtazione e Diagnostica CEDAD Univ. del Salento (Italia); Poz, Poznan Radiocarbon Laboratory (Poland); ^TL, TecnArt S.r.L., c/o Dipartimento di Fisica, Univ. degli Studi di Torino, Italia. [b]Measured radiocarbon age corrected for isotopic fractionation, calculated using the $\delta^{13}C$ (when np: not provided by the lab). It is not calendar calibrated. [c]Age dendrochronologically corrected for the $^{12}C/^{14}C$ changes in the atmosphere according to OxCal 4.3 (Bronk Ramsey, 2009) using IntCal 13 atmospheric curve (Reimer et al., 2013) and rounded to the nearest decade. Ages within curly brackets are those included in the final OxCal model for time constraints of earthquakes from SG2 trench (see also Figure S4 for stratigraphic order of samples). Asterisk on the age of sample B22S indicates that it might be post 1,950 AD.

to the Grande creek floodplain environment and represent overbank and channelized deposit, respectively. Between meters 22 and 30, a clayey deposit (unit S) overlaps the basal units A/A1; it is derived from weathering and mobilization associated to creeping and/or sudden (possibly coseismic) slump of the A/A1 units. On top of these deposits is a succession of fine to very fine-grained, scarp-derived colluvium (units C1, C2, Z, and C3). A brown soil (unit B) tops units A/A1 and unit C3 from meters 5 to 16 of the walls; it represents a significant stratigraphic marker within the sequence. On top of the paleosol B is a massive colluvial deposit mainly composed of volcanic minerals and altered small scorias (unit V), with primary volcanic layers. We do not have direct geological evidence in the area and/or other elements to associate the volcanic minerals to any eruptive history, but specific analysis focused on this purpose are in progress. Despite specific analysis focused on this purpose are in progress, mineralogy and stratigraphic context

allow us to reasonably refer this layer to the Neapolitan Yellow Tuff eruption (Campi Flegrei, Italy), dated back to 14.9 ± 0.4 ka (Deino et al., 2004). Reworked material mainly from unit V and unit A is confined within the bedrock fault zone at SG1 trench (units Cvmix, Cv, Cva, Cvb). Further colluvial (units SS1, SS2, D, C4, F, F1, M) and alluvial (units L, DS) deposits unconformably overlay the older units. At meters 40–52, the youngest units associated with faulting are characterized by anthropic and colluvial sediments (units Ant, CD, N); these are discussed in detail in section 2.2.2. The most superficial layer in SG2 is a plowed soil developed at the whole wall extent (unit H), and in SG1 are soil-sediment matrix-supported gravel and coarse-grained gravel (units Sd/Csd) deposited along the bedrock fault slope. Erosional unconformities mark abrupt transitions within the sequence, and the erosional contacts are represented with dotted lines in the trench logs (Figures 5 and 6).

The analysis of the stratigraphic and structural setting of the trenches revealed distinct event horizons (red stars in Figures 5 and 6), set based on the presence of the distinct colluvial wedges and on their faulting, on upper termination of faults, discrete increasing of vertical displacement with depth, and fissure infills. Details, time constraints of the earthquakes, and their correlation between the two trenches are discussed below.

2.2.1. SG1 Trench

SG1 trench is ~5 m long and reaches a maximum depth of 1.5 m. A complex ~2-m-wide, graben-like structure occupies the adjacent hanging wall of the bedrock fault plane (fault zone FzBr; Figure 5). Differentiated colluvial deposits, mostly consisting of fine sediment mixed to reworked, altered volcanic minerals and limestone clasts, fill in the graben, and appear offset by subvertical faults (Figure 5). Among these, unit Cva is a dark brown colluvial clay dated to 33,420–32,600 BC (sample B100N; Table 1). This age does not refer to the deposition of unit Cva but to its parent material. In fact, unit Cva is interpreted as a soil sediment derived from the denudational processes affecting the Late Pleistocene paleosol unit of comparable age (unit 3, sample QuarryCL18B; Table 1) observed within the SGF zone at the quarry (Figures 3 and 4). A dark overbank silty clay, unit A, is highly deformed within the graben and is in tectonic contact with the bedrock fault plane. This unit is overlain by Cva unit and by other colluvia that progressively deposited in newly formed graben-like structures. Among these, unit Cvmix is a displaced mixed colluvium formed of mostly yellowish red clayey silt, with an age of 10,880–10,750 BC (sample B103N; Figure 5 and Table 1). The youngest dated deposit of the faulted sequence is a colluvium of soil sediment (unit SS1), made of clayey silt with very common cherty and carbonate clasts, with an age of 8,460–8,290 BC (sample B101S; Table 1). To the west, a clear antithetic fault plane juxtaposes units Cva, and Cv with unit V, a yellowish to reddish brown clayey silt with fine volcanoclastic sand. Unit A is intensively deformed, dragged along the bedrock fault plane, and likely experienced previous displacements before to be involved in faulting along with the other younger graben units. Unit V is crossed by a series of normal faults, generally southwest side down. The fault zone (Fz3) visible at meter 0–1 is also exposed in trench SG2 (Figure 6; meter 1–2). A wedge-shaped slope deposit (unit Csd), a medium to large limestone clast-supported gravel, overlays the top of the fine-grained sequence above a gently SW dipping sharp erosional surface (Figure 5).

2.2.2. SG2 Trench

SG2 trench is ~60 m long and maximum 2.5 m deep (Figures 6, 7, and S2) and exposed geological stratigraphy (meters 0 to 40), as well as archeological remains and evidence of human modification (meters 40 to 52). Meters 1–5 of the south wall show two 40°–45° dipping main faults (fault zone Fz3) that vertically displace unit V (the eastern fault is also exposed at meter 0–1 in trench SG1; Figure 5) and unit A made of massive carbonate-free silty clay (Figures 2b and 3), and its pedogenized cover (unit A1). Basal units A/A1 are exposed along the first 40 m of the trench extent and, along with unit G (exposed between meters 32 and 39), which is a channelized deposit of clast-supported calcareous gravel, are the oldest deposits of the trench stratigraphic sequence. Dating indicates that unit A1 is 25,880–22,440 years BC (sample ISPRA1S, sample C400N; Table 1). Between meters 8 and 40 of the exposure, significant vertical displacements (up to ~1 m) occur at different location along 50° to 70° dipping normal faults, downthrowing the WSW side and slightly back-tilting the deposits. Some of these faults show minor antithetic splays at less than 1 m of distance, for which we can hypothesize a shallow depth connection. Some upper fault terminations are evident at different levels of the stratigraphic sequence, others affect the entire stratigraphy up to the base of the present soil (unit H), and generally show a discrete increasing of the displacement with depth. At places, the fine-grained units of the stratigraphic sequence (mainly units A/A1, S, and B) are characterized by structures of ductile and

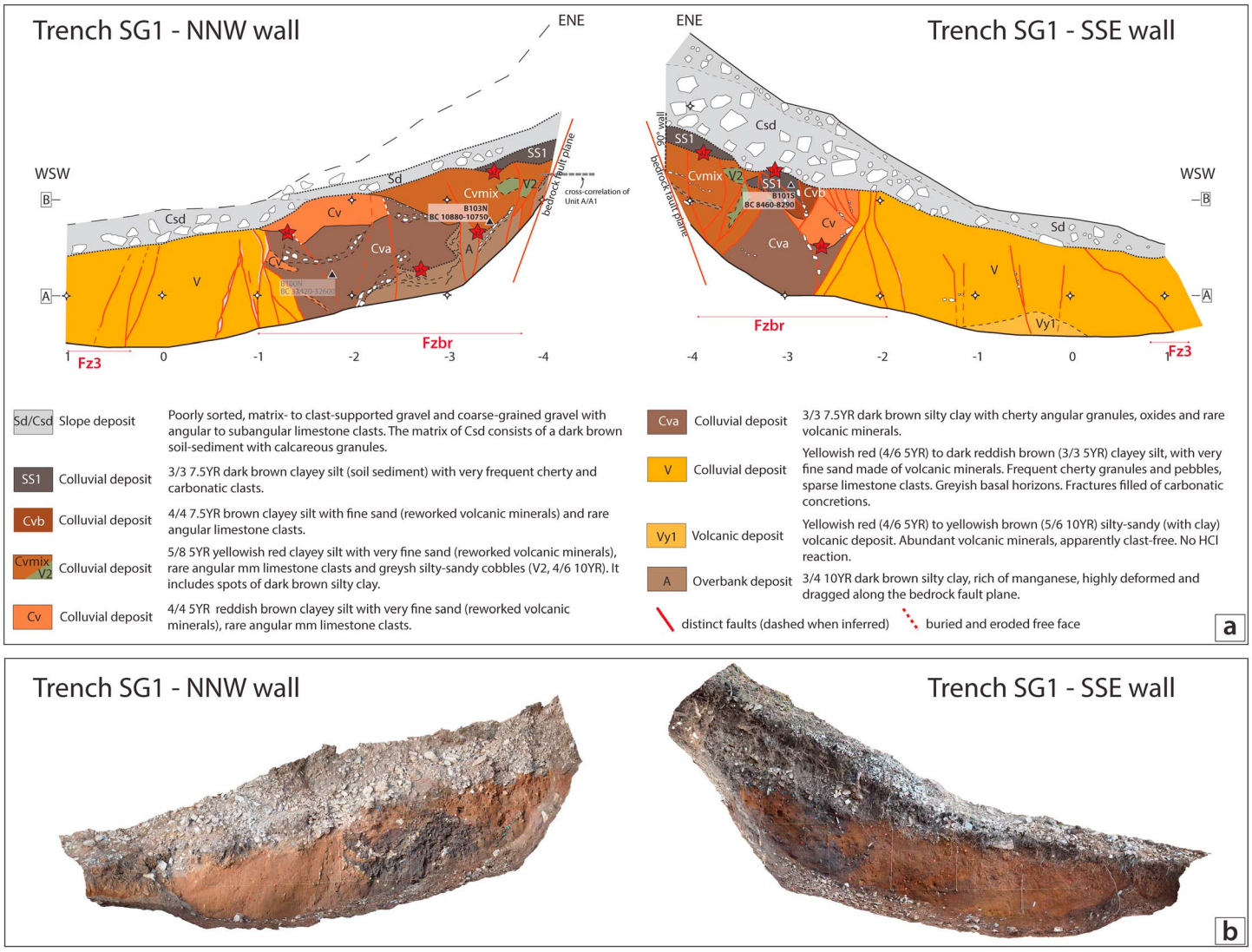

Figure 5. SG1 trench (average orientation N80). (a) Simplified logs of the trench walls from a 1:20 scale survey. Black triangles indicate dated radiocarbon samples (all bulk type; Table 1); gray label referred to age not considered reliable for the age of deposition of the unit (see section 2.1). Black bold dotted lines mark erosional and unconformity surfaces. Unit A and unit V are exposed also in SG2 trench (see Figures 6 and 7). Red stars indicate location of event horizons (ground surfaces at the time of surface faulting earthquakes). Dashed horizontal gray line in the NNW wall shows the position of unit A correlated to that in SG2 for long-term vertical slip rate evaluation. (b) Ortophotomosaics of the SG1 walls (1-m^2 grid on the wall) generated by structure-from-motion (SfM) photogrammetry from ground-based imagery.

brittle deformation (Figure S3), such as convoluted lamination, plastic intrusion, and small-scale and narrow antiforms associated with fractures and tensional faults at the hinges.

The wall exposure shows some wedge-shaped colluvial fine deposits, with sharp fault contacts and highly sheared at the fault zones (i.e., C1 to C4, from the oldest). Based on their characteristics, they are interpreted as scarp-derived colluvium and fine ponding deposits that accumulate at the downthrown fault hanging wall.

Starting from meter 40 to meter 52, the trench exposed an archeological stratigraphy ~0.5 meter below the ground surface (Figure 6). Three relic man-made walls of squared field sandstone blocks (~20 × 15 cm sized) and a weak sandy silt mortar are spaced 5 m apart. We observed wall foundations and sections (~55 cm wide) through trench floor deepening (dashed bottom line between meters 40–42 and meters 46–54 in Figure 6; see also Figure 7), which lie on a gently westward dipping surface of reddish clay (unit L), partly artificially cut. Their partial collapse is testified by the irregular profile and by the big stones laying at the same level within the anthropic colluvial deposit unit Ant in Figure 6. Abundant terracotta brick fragments, as well as portions of baked clay, charred matrix, and degraded brick debris let us hypothesize the site served as a

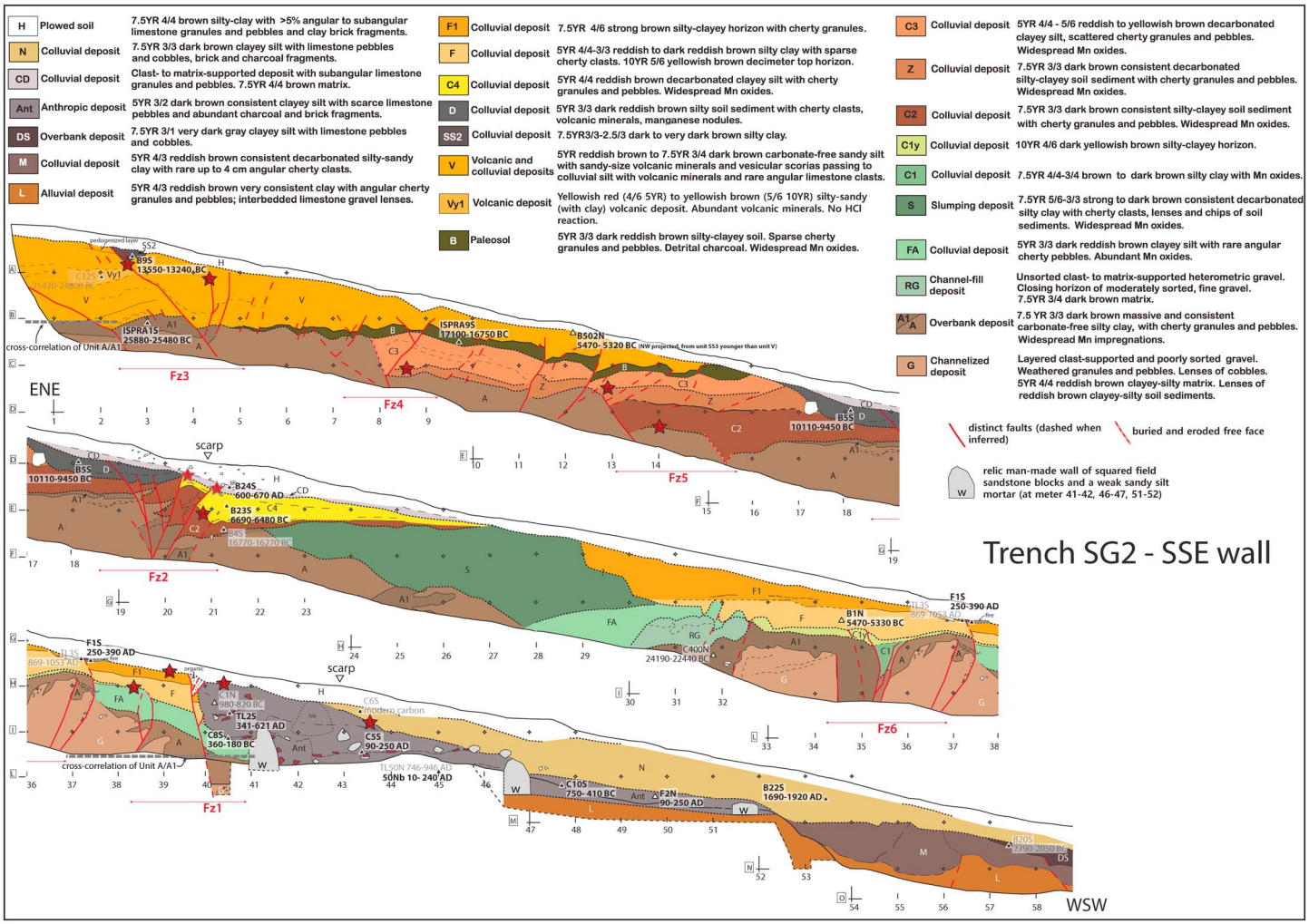

Figure 6. SG2 trench (average orientation N85). Simplified logs of the SSE trench wall from a 1:20 scale survey. Black and white triangles indicate dated radiocarbon (bulks and charcoals) and TL (brick fragments) samples collected from this wall and from the NNW wall (projected), respectively (Table 1); gray labels referred to ages not considered in the modeled age distribution in Figure 8. Black bold dotted lines mark erosional and unconformity surfaces. Red stars indicate location of event horizons (ground surfaces at the time of surface faulting earthquakes), contoured and labeled in gray when the event correlation is uncertain. Based on their time of activity, fault zones are numbered from the youngest to the oldest Fz1 to Fz6. Dashed gray lines show the correlation of units A/A1 for long-term vertical slip rate evaluation. Position of fault scarps at surface in Figure 3 is also shown (white triangles). The offset between the position of the eastern scarp and of Fz1 may be attributable to the modern modification of the ground that prevents the good expression of the fault scarp and thus its accurate location. See also Figure S2.

historical brick kiln. Due to lack of evidence, we cannot reconstruct different phases of human occupation and use of this structure, if any. However, based on the radiocarbon ages of charcoals included in unit Ant and TL dating on brick fragments, the age of occupation is post 750–410 BC (sample C10S; Table 1) and extends at least to 340–620 AD (sample TL2S; Table 1). We do not use the TL ages of sample TL3S and TL50N (Table 1) for setting the minimum age of occupation, since they are not congruent (being systematically younger by hundreds of years) with those resulting from the charcoal samples within unit Ant (samples -F2N, -F1S, -C10S, -C5S, -50Nb; Table 1 and Figure 6). These two TL samples are close to charred sediment, so that a subsequent heating of the brick fragments might be the cause of their younger ages. At meter 40, the anthropic unit Ant approaches a high-angle fault whose shear zone and hanging wall are partially removed by human activities. This fault displaces the sequence up to unit F1, below the present soil; in the lower portion, unit A is dragged into the sheared zone and displaced about 0.5 m. Since human excavations and deposits (unit Ant) replaced the faulted stratigraphy, we conclude that the anthropic stage follows the occurrence of at least one dislocation event along Fz1 up to unit F1 (see section 2.3). West of meter 43, the archeological stratigraphy is covered by a natural deposit that reaches a thickness of

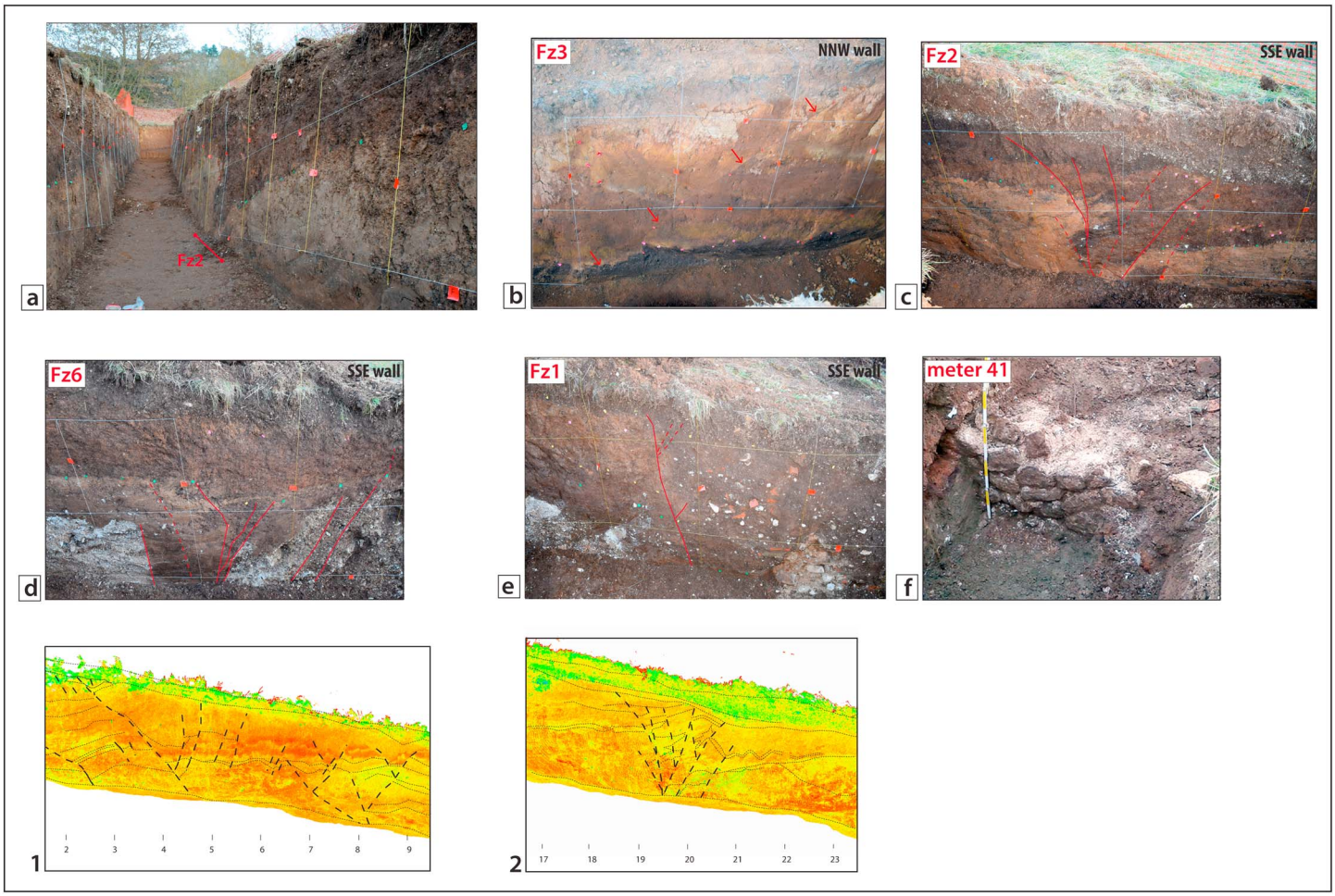

Figure 7. Pictures of the SG2 trench. (a) View to the northeast along the SG2 trench (1-m grid square for scale on the walls). (b–e) View of the main fault zones. (f) View of the stone wall after deepening at meter 41. Insets 1 and 2 show the survey of the trench wall using terrestrial laser scanning (TLS) technique (ScanStation P40; Leica Geosystem S.p.A.). The variety of colors indicates different reflectance of the materials hit by the laser. Note how this parameter highlights the different deposits and the structures, as evidenced by the comparison between inset 2 (simplified log superimposed) and picture C. See also Figures 6 and S2.

~1 m. This is an undeformed slope wash deposit made of clayey silt with pebbles and cobbles, unit N; it is the youngest one exposed in the trench (below unit H), not older than 200 years B.P. (sample B22S, 1,810–1,920 AD; Table 1). Between meters 57 and 60, unit N caps an unconformity in unit DS, dated 2,290–2,130 BC (sample B20S; Table 1). The lower portion of this trench section does not show clear and significant tectonic deformation features.

2.3. Past Surface Faulting Earthquakes and Their Ages

Trenches SG1 and SG2 across the San Giovanni fault exposed evidence of multiple faulting events in the Late Pleistocene and Holocene on at least seven fault zones (Fz1 to Fz6 and Fzbr) over a total extent of ~45 m (Figures 5 and 6). This complexity suggests that during a single earthquake multiple fault splays ruptured the surface with different amounts of slip. Based on the age of the deformed units, the discrete amount of displacement, the upper termination of faults, and the type of deposits, we recognized a total of 12 earthquake horizons at the two trenches and assigned the timeline for the activity of the main fault zones, numbered from the youngest to the oldest Fz1 to Fz6. The bedrock fault zone (Fzbr) shows repeated activity in time (Figures 5 and 6). Five events are in SG1 trench, labeled eva1 to eva5, and seven in SG2 trench, labeled evb1 to evb7 (red stars in Figures 5 and 6).

The five event horizons in SG1 trench are identified within the compound graben structure Fzbr (Figure 5) where progressive faulting and fissuring occurred and material eroded from the bedrock free faces was

trapped. Based on the relative locations of the event horizons within the stratigraphy and on fault setting, we may infer that the five events in trench SG1 likely postdate unit V (Figure 5). No dating is available for this unit; however, using the age of the underlying unit B in trench SG2 (sample SG2-ISPRA9S; Table 1), we may tentatively assess that the faulting event sequence in SG1 happened in the last 19 kyr.

We set the horizon of the oldest discrete eva5 at the base of unit Cva, filling the graben between meters −1 and −3 (Figure 5). This unit is in sharp fault contact with unit V and unconformably overlies unit A, which records a larger deformation (cumulative displacement of oldest events) and shearing along the bedrock fault plane. The age of unit Cva is unfortunately not reliable (see section 2.2.1) and cannot be used for the time constrain of the event. Successively, eva4 creates a new fissure in the graben sediment which then fills with unit Cv. A younger event, eva3, is responsible for the formation of a new narrower void between meters −3 and −4 (Figure 5). Units Cvmix and Cvb represent the fill deposits postdating this event, that is, close to 10,880–10,750 BC (sample SG1-B103N; Table 1). Then, the faulting process repeats with eva2 and the whole sequence of colluvial units within the graben structure is faulted back up to the base of unit SS1. Based on the available dating, we may set eva2 occurrence between 10,880–10,750 BC (sample SG1-B103N; Table 1) and to 8,460–8,290 BC (sample SG1-101S; Table 1). Unit SS1 appears clearly displaced in the SSE wall by the youngest event recognized in the trench, eva1. We have no time constraints for the undeformed deposits in the SG1 trench to set the minimum age of eva1; however, it occurred after 8,460–8,290 BC.

In order to constrain the age of the seven paleoearthquakes at SG2 trench, we used the OxCal 4.3 (Bronk Ramsey, 2009) program to construct a Bayesian model of conditional probability shown in Figure 8 (Bronk Ramsey, 2008; Lienkaemper and Bronk Ramsey, 2009) based on selected radiocarbon and TL ages from SG2 trench (curly bracketed values in Table 1). Our OxCal model runs a simple sequence depositional model (Bronk Ramsey, 2008) that is not depth dependent, with *Phase* and *Date* commands marking erosional events postdating the occurrence of surface faulting events and creating the probability distribution densities for each event, respectively. In detail, the adopted OxCal model refines 16 radiocarbon and one TL age distributions and provides the best estimate for event time intervals when the stratigraphic ordering of the samples is introduced (see Figure S4). In our model we do not use the three ages of SG1 from units within the complex fault zone Fzbr that is not exposed in SG2, and thus, their position within the stratigraphic sequence reconstructed for SG2 could be not fully trustworthy.

When OxCal runs a model with all the dated samples, it generates warning messages related to three samples (SG2-C12S, SG2-C1N, SG2-B4S) for very poor agreement within the sequence, providing an overall model Agreement very low, A $<$ 20% (acceptable agreement over 60%). Thus, we discarded these three samples in the final model for the following reasons: SG2-C12S and SG2-C1N (unit Vy and unit Ant, respectively) resulted out of sequence, much older than the others; SG2-B4S (unit C2) resulted too young with respect to the overlying unit (unit B, sample SG2-ISPRA9S). Moreover, we also did not insert SG2-B20S (unit DS) even though it matches the stratigraphic order (Figure S4), since it belongs to the overbank deposit of the Grande creek floodplain partly exposed at the trench edge (Figure 6) and thus not fully reliable for its stratigraphic position in the reconstructed sequence. Finally, removing these four samples from the final model (Figure 8) does not significantly change the resulting earthquake ages, but the overall Agreement index for the model becomes excellent, A = 99.8% (the OxCal code is in Text S1). In the following we will describe past faulting events and their ages (rounded to the nearest decade) inferred from the above described OxCal model.

Evidence for a distinct oldest event horizon evb7 and for its relative major vertical offsets and deformation are observed along Fz5. The surface at the time of the evb7 was the top level of units A/A1. At Fz5 the scarp-derived colluvium of unit C2 starts to be deposited in sharp contact with the fault at meter 13.5 and fill the open fissure at meter 15.5. We use the thickness of the scarp-derived colluvium of 0.8 m as minimum displacement. Similarly, evidence for the successive event, evb6, is the lower portion of colluvium unit C3, and the largest displacement occurred along Fz4. Since we do not have age constraint for the units in between the two event horizons, the probability distributions in the OxCal model of the two events partially overlap (Figure 8). The scarps produced by these two old events were eroded and the fault scarp-derived colluvium (unit C2 and unit C3) that bury the newly formed lowered areas (fault hanging wall) was partially removed. Successively, a soil developed on top (unit B) of the erosional surface. Based on the OxCal model the two distinct events, evb7 and evb6, occurred in the period between 23,780 BC and 16,850 BC (Figure 8).

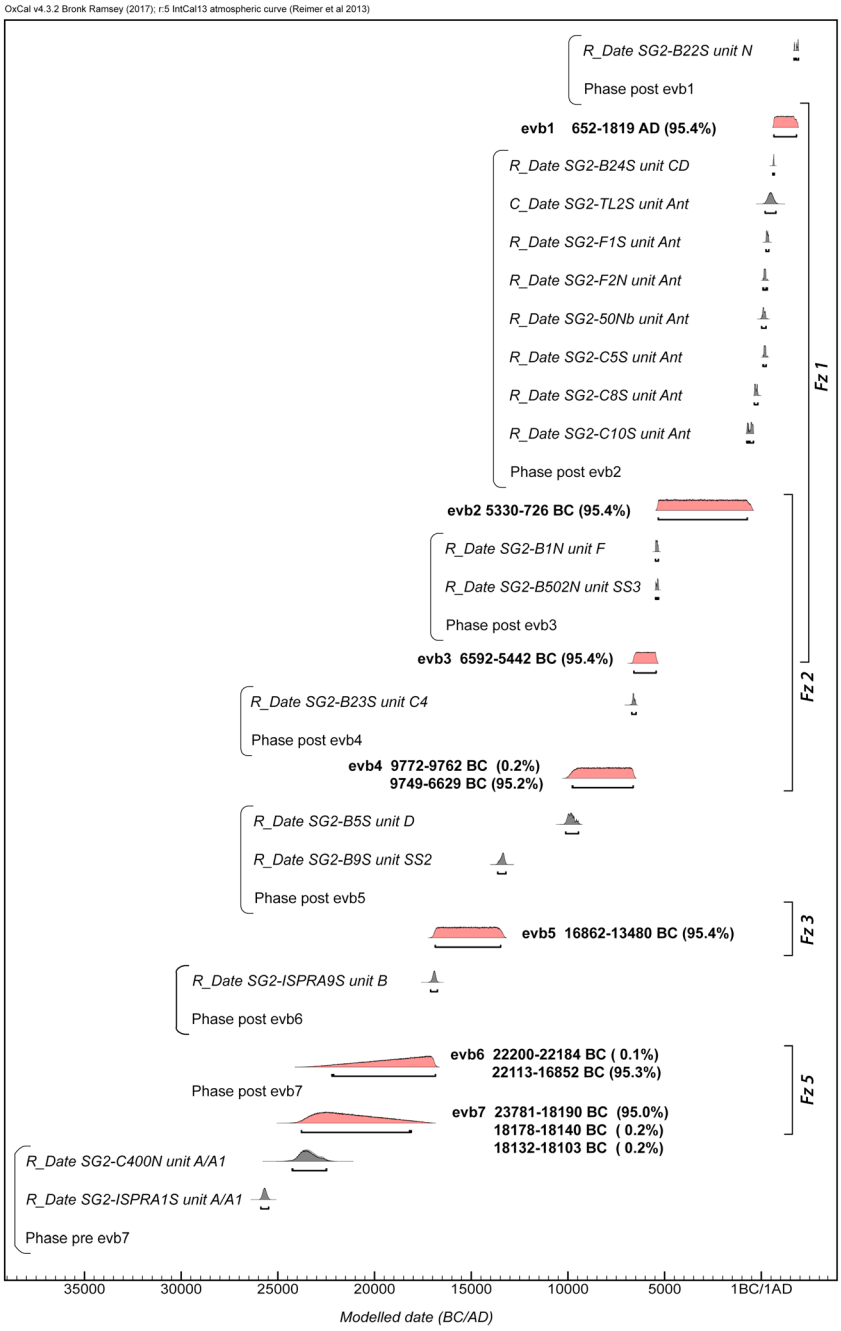

Figure 8. Calibrated and modeled age distributions of the SG2 trench radiocarbon (*R_date*) and TL (*C_Date*) samples (see also samples within curly brackets in Table 1) and paleoearthquakes by means OxCal v. 4.3 (Bronk Ramsey, 2009). Outlined gray areas show both the prior probability distribution functions of calibrated radiocarbon ages of samples and the posterior distributions, being in total overlapping thanks to an overall good model agreement (Amodel = 99.8%). OxCal's *Phase* function marks erosional events postdating the occurrence of surface faulting events. The OxCal code is supplied in Text S1. Areas labeled ev_n represent the probability distributions calculated for the paleoearthquakes. Lines below each distribution show limits of the 95.4% confidence ranges for these distributions. Earthquake ages were calculated using OxCal's *Date* function. Ages in the text are reported rounded to the nearest decade.

A younger event, evb5, displaced the units A/A1, B, and part of unit V where several faults of Fz4 and Fz3 terminate. This suggests the occurrence of evb5 during the deposition of unit V. Then, unit B predates the event, and its age indicates that evb5 occurred after 17,100 BC (SG2-ISPRA9S, unit B). In order to determine the youngest possible age for evb5, we may use the age of unit SS2 (13,550–13,240 BC) unconformably laying

on unit V and likely being the postevent colluvium. Based on net displacement of the base of unit V across Fz3 and Fz4, a minimum vertical displacement of about 0.3–0.5 m can be tentatively assigned to this event. The modeled evb5 occurrence falls within the period 16,860–13,480 BC (Figure 8).

Along fault zone Fz2, we recognize the occurrence of evb4 based on the discrete increase of the throw with depth and on the presence of unit C4 (Figures 6 and 7). This latter strongly deformed unit is a distinct scarp-derived colluvium, wedge shaped, and confined in the hanging wall of the main trace of Fz2 (i.e., colluvial wedge). The colluvial soil sediment unit D predates and unit C4 postdates the occurrence of evb4 whose event horizon is set at the base of unit C4 formed from the scarp erosion. The event evb4 occurred between 9,770 BC and 6,630 BC based on the OxCal model (Figure 8). After evb4, a further event displaced the stratigraphic sequence up to the top of unit C4 (Figure 6). Because the entire sequence is sharply truncated by an erosional surface, at this location we cannot set the event minimum age, except that is older than 670 AD (sample B24S, unit CD). We tentatively correlate this event to evb3 recognized and better time constrained in zone Fz1 (Figure 6), described in the follow. The inferred vertical displacement for each of the recognized events along Fz2 ranges between 0.3 and 0.4 m. These values are rough estimates because of the presence of multiple splays in Fz2 and of partial erosion in the footwall.

The best evidence for the event evb3 is along Fz1 at meter 38–39 (Figures 6 and 7). Here fault splays terminate below the undeformed unit F. Unit FA and the underlying unit A are vertically displaced the same amount of about 0.3 m. The age of unit F (5,470–5,330 BC, sample B1N; Table 1) postdates the event occurrence. Furthermore, as above pointed out, there is the possibility that the event found along Fz2, responsible for the dislocation of unit C4 and predating the deposition of unit CD of an unknown amount, would be timely with evb3. This correlation is based on the assumption that unit F, deposited ~10 m to the SW of Fz2, partly derived from the erosion of the paleo-surface developed on unit C4. The age of unit F is comparable to that of unit SS3 in the northern trench wall (sample B502N; Table 1 and Figure 6), a colluvial paleosol between unit CD and V, fitting with the depositional order (Figure S4). Then, we tentatively use the sample ages from unit F and unit SS3 to further constrain the event mininum age. The OxCal model sets the age of evb3 between 6,590 BC and 5,440 BC (Figure 8).

The penultimate event evb2 was observed along Fz1 at meter 40 (Figures 6, S2, and 7): unit F is fissured into the sheared zone and units F/F1 record a lower amount of displacement relative to the older unit G. The base of unit F1 is vertically displaced of ~0.4 m. The event occurrence is after 5,330 BC (sample B1N; Table 1). We do not have upper constraints for evb2 but hypothesize that is older than the human occupation (post 750–410 BC; see section 2.2.2). We suppose that faulting from evb2 occurred also along Fz2, where the sharp erosional surface on top of the overall sequence (black bold dotted line in Figure 6) forms a west facing scarp draped by the slope deposit unit CD, which is localized at the fault zone. Unit CD is the youngest undeformed unit (Figure 7). Differently from the underlying units, it is composed of clast to matrix-supported subangular gravel. In our interpretation, being unit CD so young in age (600–670 AD; sample B24S, unit CD), it is likely not an immediate postevent horizon (evb2). In fact, too much time has passed before the scarp burial and the fault scarp would have been eroded away during the interseismic period. Then the OxCal model considers the oldest age within unit Ant (sample C10S; Figure 6) and sets evb2 between 5,330 BC and 730 BC (Figure 8).

The anthropogenic impact and the natural modification (e.g., plowing and pedogenesis) of the very shallow stratigraphy prevent unequivocal recognition of the very recent fault history. However, we have some clues suggesting the occurrence of a most recent event, evb1, along Fz1 at meter 40 (Figures 6 and 7). At the uppermost portion of the fault there is a clear ~0.4-m-wide open fissure with unit F disrupted and organic-rich material infill, distinct from unit Ant. The eastern side of the fissure is marked by the imbrication of small pebbles within the matrix infill. The presence of this feature is the most robust among the clues to set the evb1 horizon. On top of the fissure is localized an inflection interpreted as coseismic scarp. This inflection is likely reduced in height (but still preserved) due to the erosional surface developed on top of unit Ant. Then, the inflection height of 0.15–0.2 m can be used as minimum estimate of the slip associated to the most recent event. Although the limited extent of the deposit prevents a straightforward correlation, the deposit at meter 37–38 containing piece of bricks and charred material is possibly a residual of the apparently offset unit Ant in the footwall of the fault zone. Unit N is a colluvium containing abundant charcoals and very small brick fragments in a clayey silt matrix, likely derived from unit Ant. It is deposited only in the downthrown side of the Fz1 and would be the postevent depositional phase. The age of evb1 would be younger than 670 AD (unit

CD) and older than the modern age of sample B22S of unit N. The OxCal model suggests an interval 650–1,820 AD (Figure 8).

Given the uncertainties, we are not able to provide a one-to-one correspondence between the events at the two trenches. However, assuming that the formation of the wide graben zone in SG1 occurred after the deposition of unit V, the oldest event recognized within Fzbr in SG1 (eva5) would postdate the age of evb5 recognized in SG2 along Fz3 that is in common between the trenches.

3. Discussion

3.1. Historical Activation of the Montereale Fault System

Our trenching data first revealed repeated reactivation of the southwestern segment of Montereale fault system, the SGF, with surface-faulting in prehistorical and historical times. We are aware of the lack of similar information for the main structure of the MFS (the CF), and our data on the SGF represents the first result for any part of the fault system.

Among the events of displacement recognized in the trench walls, the age of the inferred evb1 (650–1,820 AD) would be consistent with the southern two of the 1,703 AD main shocks (Figure 1). The 1,703 AD seismic sequence was characterized by a succession of three major events that originated on different faults from north to south (Guidoboni et al., 2018). The first main shock (I = XI, M_w 6.9, on 14 January) reliably ruptured along the Norcia fault system (NFS; Blumetti, 1995), and the southern third main shock (I = X, M_w 6.7, on 2 February) is associated to the Mount Marine fault (MMF; Moro et al., 2002, 2016) and, subordinately, to the northern section of the Paganica-San Demetrio fault system (PSDFS; Galli et al., 2011; Figure 1). Of course, age constraints from trenching data cannot discriminate between events so close in time; however, based on the intensity values, the macroseismic area (Guidoboni et al., 2018) would indicate the MFS as a candidate source of the second main shock, I = VIII (*M*6.0) on 16 January 1703. According to our hypothesis for evb1, the amount of displacement is about 0.2 m. This value estimated on one splay, although it may represent a minimum in the case of simultaneous additional slip along the other splays of the Montereale system, would be expected for an earthquake of $M_w \geq 6.0$ (Stirling et al., 2013; Wesnousky, 2008). At the same time, we cannot exclude that surface breaking (sympathetic rupture) repeated along the MFS during the third event of the 1,703 sequence (on 2 February), and then it would represent the cumulative displacement of two events close in time.

The MFS lies at the juncture of the epicentral areas of two recent major earthquake sequences: the 2009 L'Aquila (Chiaraluce et al., 2011; Valoroso et al., 2013) and the 2016–2017 central Italy (Chiaraluce et al., 2017; see also Figure 1). In 2009, two main sources were identified as the earthquake faults, the Paganica fault rupturing at surface with M_w 6.1 on 6 April (Cinti et al., 2011; EMERGEO Working Group, 2010), and the southern section of the Laga Mountains fault system (LMFS) rupturing but remaining blind with a M_w 5.4 on 9 April (Atzori et al., 2009; Chiaraluce et al., 2011; Valoroso et al., 2013). Seven years later, a new seismic sequence originated to the north; on 24 August (M_w 6.0) and later on 30 October 2016 (M_w 6.5) with surface ruptures along the Mount Vettore-Mount Bove fault system (Civico et al., 2018; EMERGEO Working Group, 2016; Pucci et al., 2017; Villani et al., 2018), and on 18 January 2017 the southernmost and contiguous LMFS ruptured again, partially overprinting the 9 April 2009 (M_w 5.4) event (Figure 1).

The Montereale fault system, subparallel to the LMFS and located at a distance of~10–15 km to the west in its hanging wall (Figure 1), lies within the aftershock area of the 2009 (dark blue dots) and 2016–2017 sequences (black and red dots, respectively; Figure S5). The hypocentral distributions of the two aftershock sequences define the presence of the master fault plane corresponding to the LMFS (Gruppo di Lavoro INGV sul Terremoto in centro Italia, 2017; see Figure S5). An additional 40°–65° SW dipping alignment of sparse hypocenters west of the LMFS is consistent with the location and the geometry of the MFS fault plane measured on the field (~55° WSW dipping plane; Figure S5). Despite the small number and size ($M_w \leq 4.0$) of the events, they suggest that the MFS activated at depths between 3 and 12 km; this was already pointed out by Lavecchia et al. (2012) solely based on the 2009 aftershocks. Therefore, the MFS is a source physically independent at the surface and at depth as well, not merging into the master fault (i.e., LMFS), and it may have played a role in the stress transfer process in both of the seismic crisis. It is worth noting that the activation of synthetic fault planes (e.g., the Norcia fault system) in the hanging wall of the Mount Vettore-Mount Bove

earthquake fault system is particularly well defined by the 2016 hypocenters in the Castelluccio and Norcia area, north of Montereale (Figures 1 and S5; Civico et al., 2018; Ferrario & Livio, 2018; Gruppo di Lavoro INGV sul terremoto in centro Italia, 2017; Villani et al., 2018).

3.2. Fault Parameters

Based on previous works on the Montereale area (Chiarini et al., 2014; Civico et al., 2016; Lavecchia et al., 2012) and on the present trenching study across one splay of the MFS, that is, San Giovanni fault, we summarize the following fault parameters.

Length and strike: the subparallel CF and SGF traces run with an average strike of N145° for ~12 km at the base of the NW-SE striking Montereale basin-bounding mountain front and ~8 km along the base of the southwestern slope of the Monte Mozzano ridge, respectively (Figure 2a). The maximum length for the MFS is ~20 km considering its possible continuation to the north with the adjacent ~7-km-long Configno fault (Figure 1). The MFS length values at surface are in agreement with those resulting from the empirical relationships for normal faulting between surface rupture length and average surface displacement (Wells & Coppersmith, 1994; Wesnousky, 2008), ranging from 18 to 21 km.

Late Pleistocene to Holocene vertical slip rate: unit A/A1 has subhorizontal attitude (overbank deposit), it outcrops at the base of the SG2 trench for most of the extent (Figures 6, 7, and S2), and is also visible in the hanging wall of Fzbr in SG1, dragged into the plane (Figure 5). This provides an opportunity to estimate a minimum cumulative vertical displacement across all the fault zones in the main hanging wall exposed in the trench walls of about 9 m (for unit correlation, see dashed gray lines in Figure S2). Considering the age of unit A1 (sample C400, sample ISPRA1S), this amount of displacement occurred in 27,830–24,390 years and gives a Late Pleistocene to Holocene vertical slip rate at the trench site of at least 0.3–0.4 mm/yr. This value is a minimum since trenches do not cross the main bedrock fault and some slip is likely missing.

Recurrence interval: seven surface rupturing events were recognized in the SGF trenches in the time span of 26–28 kyr (minimum and maximum age of unit A). This provides a mean recurrence interval for surface faulting events of 3,850 ± 150 years. This interval is a maximum estimate due to the presence of several erosional surfaces throughout the depositional sequence that may have removed event evidence.

Slip per event: the throws associated to the individual events vary between 0.15 and 0.8 m. These values were measured along the relative main earthquake fault trace and represent minimum estimates as based on wedge thickness and partially eroded coseismic scarp. Moreover, they are probably minima since when summed for the seven events, they do not reach the amount of Holocene cumulative vertical displacement across all the fault zones in the main hanging wall (about 9 m; Figure S2). This latter estimate yields an average slip per event of ~1.3 m. It is possible that minor deformation for a specific event occurred also along the other numerous fault splays of the overall fault zone exposed in the trenches. This amount of slip would be missing in our estimation, as well as possible plastic deformation in clay deposits, thus explaining the difference between the estimates. Finally, the data collected are relative to a section of the MFS and does not include slip on the CF strand.

Finally, based on our analysis of the long-term expression (Civico et al., 2016) and of trenching data (this paper), we recognize the MFS as an individual source within a dense array of adjacent active faults, and suggest that it is capable of producing surface faulting earthquakes of *M* equal and larger than 6.0.

The multisegment setting and the maximum extent of the MFS, as well as event displacements, recurrence, and slip rates values, are common characteristics of other active fault systems in the central Apennines. For example, the fault systems recently activated north and south of the MFS, the Mount Vettore-Mount Bove (2016 earthquake sequence) and the Paganica-S. Demetrio (2009 earthquake sequence; Figure 1), are both characterized by multiple, subparallel, partially overlapping segments, with a total surface length ranging from 20 to 30 km. The slip found for paleoearthquakes along the Paganica-S. Demetrio varies from 0.15 to 0.8 m (Cinti et al., 2011, and references therein), and for the Mount Vettore-Mount Bove is a minimum of 0.45 m (Galadini & Galli, 2003). As for the paleoseismologically derived Holocene slip rates, minimum vertical values of 0.11–0.36 mm/yr for the Mount Vettore-Mount Bove system (Galadini & Galli, 2003), and average dip-slip rate of ~0.3–0.4 mm/yr for the Paganica-S. Demetrio fault system (Cinti et al., 2011, and references therein) are found. The recurrence interval from trenching is no longer than 4,690 years for the Mount Vettore fault, while intervals varying in time from 500 to 2,000 years were estimated with the trench

campaign along the Paganica-S. Demetrio fault system (Cinti et al., 2011). With respect to the Laga Mountains fault system, east of and subparallel to the MFS, more uncertain data are available from trenching (Galadini & Galli, 2003): a mimimum of 0.12 mm/yr Holocene slip rate and a recurrence interval less than 7,570 years (Galadini & Galli, 2003).

4. Conclusion

On the basis of the paleoseismological investigation conducted at the San Giovanni fault segment we obtained the first reconstruction of the seismic history of the Montereale fault system. We estimate 0.15 to 0.8 m of minimum throw per event and a minimum Late Pleistocene slip rate of 0.3–0.4 mm/yr.

The main results of this study can be summarized in the following points:

1. A sequence of seven distinct paleoevents were recognized in the fault zone at the hanging wall of the SGF bedrock fault plane. They are characterized by a similar style of deformation, occurring on west-southwest side down faults. Multiple faults ruptured with the same individual event;
2. The most recent event (evb1) on the MFS possibly occurred at 650–1,820 AD, and thus could be the causative rupture for the historical 16 January 1703 earthquake (*M*6.0). We inferred ~0.2 m of minimum displacement in the evb1, which is consistent with the earthquake magnitude;
3. The MFS is an individual earthquake source and has the capability to produce surface faulting earthquakes of *M* equal and larger than 6.0. The resulting slip rate is fully comparable with those known for faults in central Apennines. It cannot be excluded a multifault rupture associated to a large earthquake, involving simultaneously the MFS and the adjacent/stepping faults.

The historical and recent paleoseismic history of the central Apennines reveals the high susceptibility of this region to complex seismic sequences on numerous faults and fault segments. Conscious that these scenarios will repeat in the future, the recognition of the seismic rupture history through additional trenches along the MFS and along the neighboring faults is a critical path for accurate segmentation modeling and for understanding possible rupture scenarios. Moreover, there is a strong need for systematic prevention plans based on detailed local seismic hazard evaluations such as surface faulting hazard, and our study on the MFS points toward that direction.

Acknowledgments
We are grateful to those who were occasionally involved in the research and trenching activity (Guido Ventura, Vincenzo Sapia, Riccardo De Ritis, Paola Del Carlo, Alessio Di Roberto). Thanks to the Istituto Diocesano del Sostentamento del Clero and to Claudio Cherubini for having allowed the trenching on their land. We also thank Vincenzo Torrieri from Soprintendenza Archeologia, Belle Arti e Paesaggio, for the collaboration and the fruitful discussion. INGV researchers developed the activities related to SfM photogrammetry at the site and the Terrestrial Laser Scanning survey of the trench walls. As regards the latter, we are grateful to the specialists of the Leica Geosystems S.p.A. for providing equipment, expertise, and full availability to collaborate with the INGV. The data and the analysis of the fault zone at the Quarry wall were conducted by the ISPRA researchers in 2005. We thank the Editor Assistant and the reviewers for their comments. We are particularly grateful to Christopher DuRoss whose constructive criticisms and suggestions contributed to improve the original manuscript. This work was financially supported by the MIUR (Italian Ministry of Education, University and Research) project "FIRB Abruzzo—High-resolution analyses for assessing the seismic hazard and risk of the areas affected by the 6 April 2009 earthquake," ref. RBAP10ZC8K_005. Data used in the present paper are available in Table and in the cited references.

References

Atzori, S., Hunstad, I., Chini, M., Salvi, S., Tolomei, C., Bignami, C., et al. (2009). Finite fault inversion of DInSAR coseismic displacement of the 2009 L'Aquila earthquake (central Italy). *Geophysical Research Letters*, *36*, L15305. https://doi.org/10.1029/2009GL039293

Blumetti, A. M. (1995). Neotectonic investigations and evidence of paleoseismicity in the epicentral area of the January–February 1703, central Italy, earthquakes. In L. Serva & D. B. Slemmons (Eds.), *Perspectives in Paleoseismology*, *Ass. of Eng. Geologists, Spec. Publ.* (Vol. 6, pp. 83–100).

Blumetti, A. M., Dramis, F., & Michetti, A. M. (1993). Fault-generated mountain fronts in the central Apennines (central Italy): Geomorphological features and seismotectonic implications. *Earth Surface Processes and Landforms*, *18*(3), 203–223. https://doi.org/10.1002/esp.3290180304

Blumetti, A. M., & Guerrieri, L. (2007). Fault-generated mountain fronts and the identification of fault segments: Implications for seismic hazard assessment. *Bollettino della Società Geologica Italiana (Italian Journal of Geoscience)*, *126*(2), 307.

Boncio, P., Lavecchia, G., & Pace, B. (2004). Defining a model of 3D seismogenic sources for seismic hazard assessment applications: The case of central Apennines (Italy). *Journal of Seismology*, *8*(3), 407–425. https://doi.org/10.1023/B:JOSE.0000038449.78801.05

Bronk Ramsey, C. (2008). Deposition models for chronological records. *Quaternary Science Reviews*, *27*(1–2), 42–60.

Bronk Ramsey, C. (2009). Bayesian analysis of radiocarbon dates. *Radiocarbon*, *51*(01), 337–360. https://doi.org/10.1017/S0033822200033865

Cavinato, G. P., & De Celles, P. G. (1999). Extensional basins in the tectonically bimodal central Apennines fold-thrust belt, Italy: Response to corner flow above a subducting slab in retrograde motion. *Geology*, *27*(10), 955–958. https://doi.org/10.1130/0091-7613(1999)027<0955:EBITTB>2.3.CO;2

Cello, G., Mazzoli, S., & Tondi, E. (1998). The crustal fault structure responsible for the 1703 earthquake sequence of central Italy. *Journal of Geodynamics*, *26*(2–4), 443–460. https://doi.org/10.1016/S0264-3707(97)00051-3

Cello, G., Mazzoli, S., Tondi, E., & Turco, E. (1997). Active tectonics in the central Apennines and possible implications for seismic hazard analysis in peninsular Italy. *Tectonophysics*, *272*(1), 43–68. https://doi.org/10.1016/S0040-1951(96)00275-2

Centamore, E., Adamoli, L., Berti, D., Bigi, S., Casnedi, R., Cantalamessa, G., et al. (1992). Carta geologica dei bacini della Laga e del Cellino e dei rilievi carbonatici circostanti (Marche meridionali, Lazio nord-orientale, Abruzzo settentrionale). Scala 1:100.000. Firenze, SELCA.

Chiarabba, C., Jovane, L., & Di Stefano, R. (2005). A new view of Italian seismicity using 20 years of instrumental recordings. *Tectonophysics*, *305*, 251–268.

Chiaraluce, L., Di Stefano, R., Tinti, E., Scognamiglio, L., Michele, M., Casarotti, E., et al. (2017). The 2016 central Italy seismic sequence: A first look at the mainshocks, aftershocks, and source models. *Seismological Research Letters*, *88*, 757–771. https://doi.org/10.1785/0220160221

Chiaraluce, L., Valoroso, L., Piccinini, D., Di Stefano, R., & De Gori, P. (2011). The anatomy of the 2009 L'Aquila normal fault system (central Italy) imaged by high resolution foreshock and aftershock locations. *Journal of Geophysical Research*, *116*, B12311. https://doi.org/10.1029/2011JB008352

Chiarini, E., La Posta, E., Cifelli, F., D'Ambrogi, C., Eulilli, V., Ferri, F., et al. (2014). A multidisciplinary approach to the study of the Montereale Basin (central Apennines, Italy). *Rendiconti Lincei*, *25*(Suppl. 2), 177–188. https://doi.org/10.1007/s12210-014-0311-3

Cinti, F. R., Pantosti, D., De Martini, P. M., Pucci, S., Civico, R., Pierdominici, S., et al. (2011). Evidence for surface faulting events along the Paganica Fault prior to the April 6, 2009 L'Aquila earthquake (central Italy). *Journal of Geophysical Research*, *116*, B07308. https://doi.org/10.1029/2010JB007988

Civico, R., Blumetti, A. M., Chiarini, E., Cinti, F. R., La Posta, E., Papasodaro, F., et al. (2016). Traces of the active Capitignano and San Giovanni Faults (Abruzzi Apennines, Italy). *Journal of Maps*, *12*(sup1), 453–459. https://doi.org/10.1080/17445647.2016.1239229

Civico, R., Pucci, S., Villani, F., Pizzimenti, L., De Martini, P. M., Nappi, R., & the Open EMERGEO Working Group (2018). Surface ruptures following the 30 October 2016 M_w 6.5 Norcia earthquake, central Italy. *Journal of Maps*, *14*(2), 151–160. https://doi.org/10.1080/17445647.2018.1441756

D'Agostino, N., Avallone, A., Cheloni, D., D'Anastasio, E., & Mantenuto, S. (2008). Active tectonics of the Adriatic region form GPS and earthquake slip vectors. *Journal of Geophysical Research*, *113*, B12413. https://doi.org/10.1029/2008JB005860

D'Agostino, N., Mantenuto, S., D'Anastasio, E., Giuliani, R., Mattone, M., Calcaterra, S., et al. (2011). Evidence for localized active extension in the central Apennines (Italy) from Global Positioning System observations. *Geology*, *39*(4), 291–294. https://doi.org/10.1130/G31796.1

Deino, A. L., Orsi, G., De Vita, S., & Piochi, M. (2004). The age of the Neapolitan yellow tuff caldera-forming eruption (Campi Flegrei caldera-Italy) assessed by $^{40}Ar/^{39}Ar$ dating method. *Journal of Volcanology and Geothermal Research*, *133*(1-4), 157–170. https://doi.org/10.1016/S0377-0273(03)00396-2

Devoti, R., Esposito, A., & Pietrantonio, G. (2011). Evidence of large scale deformation patterns from GPS data in the Italian subduction boundary. *Earth and Planetary Science Letters*, *311*(3–4), 230–241. https://doi.org/10.1016/j.epsl.2011.09.034

EMERGEO Working Group (2010). Evidence for surface rupture associated with the M_w 6.3 L'Aquila earthquake sequence of April 2009 (Central Italy). *Terra Nova*, *22*(1), 43–51. https://doi.org/10.1111/j.1365-3121.2009.00915

EMERGEO Working Group (2016). Coseismic effects of the 2016 Amatrice seismic sequence: First geological results. *Annals of Geophysics*, *59*. Fast Track 5. https://doi.org/10.4401/AG-7195

Faure Walker, J. P., Roberts, G. P., Sammonds, P. R., & Cowie, P. (2010). Comparison of earthquake strain rates over 102 to 104 year timescales: Insights into variability in the seismic cycle in the central Apennines, Italy. *Journal of Geophysical Research*, *115*, B10418. https://doi.org/10.1029/2009JB006462

Ferrario, M. F., & Livio, F. (2018). Characterizing the distributed faulting during the 30 October 2016, central Italy earthquake: A reference for fault displacement hazard assessment. *Tectonics*, *37*, 1256–1273. https://doi.org/10.1029/2017TC004935

Festa, A. (2005). Geometrie e meccanismi di raccorciamento nel settore meridionale del Bacino marchigiano (Monte Gorzano, Appennino centrale). *Bollettino della Società Geologica Italiana*, *44*, 41–51.

Galadini, F., & Galli, P. (2000). Active tectonics in the central Apennines (Italy)—Input data for seismic hazard assessment. *Natural Hazards*, *22*(3), 225–268. https://doi.org/10.1023/A:1008149531980

Galadini, F., & Galli, P. (2003). Paleoseismology of silent faults in the central Apennines (Italy): The Mt. Vettore and Laga Mts. Faults. *Annals of Geophysics*, *46*, 5.

Galli, P., Galadini, F., & Calzoni, F. (2005). Surface faulting in Norcia (central Italy): A "paleoseismological perspective". *Tectonophysics*, *403*(1–4), 117–130. https://doi.org/10.1016/j.tecto.2005.04.003

Galli, P., Giaccio, B., Messina, P., Peronace, E., & Zuppi, G. M. (2011). Palaeoseismology of the L'Aquila faults (central Italy, 2009, M_w 6.3 earthquake): implications for active fault linkage. *Geophysical Journal International*. https://doi.org/10.1111/j.1365-246X.2011.05233.x

Gruppo di Lavoro INGV sul terremoto di Visso (2016). Rapporto di sintesi sul Terremoto di Visso Ml 5.9 del 26 ottobre 2016 (Italia Centrale). https://doi.org/10.5281/zenodo.163818

Gruppo di Lavoro INGV sul terremoto in centro Italia (2016). Summary report on the October 30, 2016 earthquake in central Italy M_w6.5. https://doi.org/10.5281/zenodo.166238

Gruppo di Lavoro INGV sul Terremoto in centro Italia (2017). Relazione sullo stato delle conoscenze sulla sequenza sismica in centro Italia 2016–2017 (aggiornamento al 2 Febbraio 2017). https://doi.org/10.5281/zenodo.267984

Guidoboni, E., Ferrari, G., Mariotti, D., Comastri, A., Tarabusi, G., Sgattoni, G., et al. (2018). CFTI5Med, Catalogo dei Forti Terremoti in Italia (461 A.C.–1997) e nell'area Mediterranea (760 A.C.–1500), Istituto Nazionale di Geofisica e Vulcanologia (INGV). Retrieved from http://storing.ingv.it/cfti/cfti5/

INGV working group on the Amatrice earthquake (2016). Second summary report on the *M*6.0 Amatrice earthquake of August 24, 2016 (central Italy). https://doi.org/10.5281/zenodo.166241

Lavecchia, G., Ferrarini, F., Brozzetti, F., De Nardis, R., Boncio, P., & Chiaraluce, L. (2012). From surface geology to aftershock analysis: Constraints on the geometry of the L'Aquila 2009 seismogenic fault system. *Italian Journal of Geosciences*, *131*(3), 330–347.

Lienkaemper, J. J., & Bronk Ramsey, C. (2009). OxCal: Versatile tool for developing paleoearthquake chronologies—A primer. *Seismological Research Letters*, *80/3*.

Moro, M., Bosi, V., Galadini, F., Galli, P., Giaccio, B., Messina, P., & Sposato, A. (2002). Analisi paleosismologiche lungo la faglia del M. Marine (alta valle dell'Aterno): Risultati preliminari. *Il Quaternario*, *15*, 267–278.

Moro, M., Falcucci, E., Gori, S., Saroli, M., & Galadini, F. (2016). New paleoseismic data across the Mt. Marine Fault between the 2016 Amatrice and 2009 L'Aquila seismic sequences (central Apennines). *Annals of Geophysics*, *59*. Fast Track 5. https://doi.org/10.4401/ag-7260

Pierantoni, P., Deiana, G., & Galdenzi, S. (2013). Stratigraphic and structural features of the Sibillini Mountains (Umbria-Marche Apennines, Italy). *Italian Journal of Geosciences*, *132*(3), 497–520.

Pucci, S., De Martini, P. M., Civico, R., Villani, F., Nappi, R., Ricci, T., et al. (2017). Coseismic ruptures of the 24 August 2016, M_w 6.0 Amatrice earthquake (central Italy). *Geophysical Research Letters*, *44*, 2138–2147. https://doi.org/10.1002/2016GL071859

Pucci, S., Villani, F., Civico, R., Pantosti, D., Del Carlo, P., Smedile, A., et al. (2015). Quaternary geology of the middle Aterno Valley, 2009 L'Aquila earthquake area (Abruzzi Apennines, Italy). *Journal of Maps*, *11*(5), 689–697. https://doi.org/10.1080/17445647.2014.927128

Reimer, P. J., Bard, E., Bayliss, A., Beck, J. W., Blackwell, P. G., Bronk Ramsey, C., et al. (2013). IntCal13 and Marine13 radiocarbon age calibration curves 0–50,000 years cal BP. *Radiocarbon*, *55*(04), 1869–1887. https://doi.org/10.2458/azu_js_rc.55.16947

Stirling, M., Goded, T., Berryman, K., & Litchfield, N. (2013). Selection of earthquake scaling relationships for seismic-hazard analysis. *Bulletin of the Seismological Society of America*, *103*(6), 2993–3011. https://doi.org/10.1785/0120130052

Valoroso, L., Chiaraluce, L., Piccinini, D., Di Stefano, R., Schaff, D., & Waldhauser, F. (2013). Radiography of a normal fault system by 64,000 high-precision earthquake locations: The 2009 L'Aquila (central Italy) case study. *Journal of Geophysical Research: Solid Earth*, *118*, 1156–1176. https://doi.org/10.1002/jgrb.50130

Vezzani, L., & Ghisetti, F. (1998). Carta Geologica dell'Abruzzo, Scala 1:100,000. S.EL.CA., Firenze.

Villani, F., Civico, R., Pucci, S., Pizzimenti, L., Nappi, R., De Martini, P. M., & the Open EMERGEO Working Group (2018). A database of the coseismic effects following the 30 October 2016 Norcia earthquake in central Italy. *Science Data*, *5*, 180049. https://doi.org/10.1038/sdata.2018.49

Wells, D. L., & Coppersmith, K. J. (1994). New empirical relationships among magnitude, rupture length, rupture width, rupture area, and surface displacement. *Bulletin of the Seismological Society of America*, *84*, 974–1002.

Wesnousky, S. G. (2008). Displacement and geometrical characteristics of earthquake surface ruptures: Issues and implications for seismic-hazard analysis and the process of earthquake rupture. *Bulletin of the Seismological Society of America*, *98*(4), 1609–1632. https://doi.org/10.1785/0120070111